REFERENCES AND NOTES

1. G. Binnig, C. F. Quate, C. Gerber, *Phys. Rev. Lett.* **56**, 930 (1986).
2. G. Binnig, C. Gerber, E. Stoll, T. R. Albrecht, C. F. Quate, *Europhys. Lett.* **3**, 1281 (1987).
3. G. Binnig, *Ultramicroscopy* **42–44**, 7 (1992).
4. J. Frommer, *Angew. Chem. Int. Ed. Engl.* **31**, 1298 (1992).
5. D. Rugar and P. K. Hansma, *Phys. Today* **43** (no. 10), 23 (1990).
6. O. Marti, B. Drake, P. K. Hansma, *Appl. Phys. Lett.* **51**, 484 (1987).
7. B. Drake *et al.*, *Science* **243**, 1586 (1989).
8. W. Häberle, J. K. H. Hörber, G. Binnig, *J. Vac. Sci. Technol.* **B9**, 1210 (1991).
9. W. Häberle, J. K. H. Hörber, F. Ohnesorge, D. P. E. Smith, G. Binnig, *Ultramicroscopy* **42–44**, 1161 (1992).
10. S. Manne, P. K. Hansma, J. Massie, V. B. Elings, A. A. Gewirth, *Science* **251**, 183 (1991).
11. M. Radmacher, R. W. Tillmann, M. Fritz, H. E. Gaub, *Science* **257**, 1900 (1992).
12. D. Sarid, *Scanning Force Microscopy* (Oxford Univ. Press, New York, 1991).
13. G. Friedbacher, P. K. Hansma, E. Ramli, G. D. Stucky, *Science* **253**, 1261 (1991); P. E. Hillner, S. Manne, A. J. Gratz, P. K. Hansma, *Ultramicroscopy* **42–44**, 1387 (1992); P. E. Hillner, A. J. Gratz, S. Manne, P. K. Hansma, *Geology* **20**, 359 (1992); A. J. Gratz, P. E. Hillner, P. K. Hansma, *Geochim. Cosmochim. Acta* **57**, 491 (1993); P. E. Hillner, S. Manne, A. J. Gratz, P. K. Hansma, *Faraday Discuss. Chem. Soc.*, in press.
14. A. L. Rachlin, G. S. Henderson, M. C. Goh, *Am. Mineral.* **77**, 904 (1992).
15. F. Ohnesorge and G. Binnig, unpublished results.
16. F. Ohnesorge *et al.*, *Ultramicroscopy* **42–44**, 1236 (1992).
17. We used cantilevers made of crystalline silicon ("Ultralevers") from Park Scientific Instruments, Sunnyvale, CA 94089, which were 95 μm in length and 0.6 μm in thickness. The measured resonance frequencies of the cantilevers we used were within 2 to 3% of the nominal value of 77 kHz. The approximate tolerance of their normal spring constants is thus ~10%. See also J. P. Cleveland, S. Manne, D. Bocek, P. K. Hansma, *Rev. Sci. Instrum.* **64** (2), 403 (1993).
18. R. W. G. Wyckoff, *Crystal Structures* (Wiley, New York, 1964).
19. G. M. McClelland, R. Erlandsson, S. Chiang, in *Review of Progress in Quantitative Non-Destructive Evaluation*, D. O. Thompson and D. E. Chimenti, Eds. (Plenum, New York, 1987), vol. 6b, pp. 1307–1314
20. A. L. Weisenhorn, P. K. Hansma, T. R. Albrecht, C. F. Quate, *Appl. Phys. Lett.* **54**, 2651 (1989).
21. J. Israelachvili, *Intermolecular and Surface Forces* (Academic Press, London, ed. 2, 1991).
22. U. Hartmann, *Phys. Rev. B* **43**, 2404 (1991).
23. J. E. Dzyaloshinskii, E. M. Lifshitz, L. B. Pitaevskii, *Adv. Phys.* **10**, 165 (1961).
24. A. L. Weisenhorn, P. Maivald, H.-J. Butt, P. K. Hansma, *Phys. Rev. B* **45** (19), 11226 (1992).
25. S. A. Joyce and J. E. Houston, *Rev. Sci. Instrum.* **62**, 710 (1991).
26. F. F. Abraham, I. P. Batra, S. Ciraci, *Phys. Rev. Lett.* **60**, 1314 (1988); S. A. C. Gould, K. Burke, P. K. Hansma, *Phys. Rev. B* **40**, 5363 (1989); P. Rasch, W. M. Heckl, H. W. Deckman, W. Häberle, *Mater. Res. Soc. Symp. Proc.* **233**, 287 (1991).
27. J. H. Hoh, J. P. Cleveland, C. B. Prater, J.-P. Revel, P. K. Hansma, *J. Am. Chem. Soc.* **114**, 4917 (1991).
28. F. J. Giessibl, *Phys. Rev. B*, **45**, 13815 (1992).

29. We thank D. P. E. Smith, W. Häberle, and W. M. Heckl for their help and advice, as well as J. K. H. Hörber, D. Wolf, and G. Dollinger for many inspiring discussions.

Field-Flow Fractionation: Analysis of Macromolecular, Colloidal, and Particulate Materials

J. Calvin Giddings

Field-flow fractionation (FFF) is a family of flexible elution techniques capable of simultaneous separation and measurement. Its sample domain extends across a broad macromolecular-colloidal-particulate continuum from about 1 nanometer to more than 100 micrometers and incorporates both simple and complex macromaterials of biological, biomedical, industrial, and environmental relevance. Complex materials are separated into components to simplify measurement. Component properties measurable by FFF include mass, size, density, charge, diffusivity, and thickness of adsorbed layers. When characterization by these properties is inadequate, other measurement tools can be readily coupled to FFF, either off-line or on-line, by virtue of its flow-elution operation. This article describes the principles and major subtechniques of the FFF family along with application of its measurement and separative capabilities.

Field-flow fractionation is a relatively new family of techniques designed to disentangle and probe the physical and compositional structure of complex macromolecular, colloidal, and particulate materials (*1–10*). These tasks are approached through broad capabilities for both separation and measurement. Species can be separated in the 10^5-fold size range from $\sim 10^{-3}$ to 10^2 μm. The separation occurs by differential retention in a stream of liquid flowing through a thin channel. The separated components are eluted one at a time into a detector. The observed retention time t_r is related (often rigorously) to various physicochemical properties of the retained species; the measurement of t_r values can therefore yield these properties for each fractionated component. If this characterization is not sufficient, fractions can be readily collected and further examined by microscopy, light scattering, elemental analysis, subsequent FFF steps, and so on. The additional characterization can frequently be made on-line by directly coupling FFF and other measurement devices.

Separation has long been a key step in characterizing complex polydisperse macromaterials. Through separation, complex samples are simplified by division into digestible units for measurement and analysis. The recent explosive growth in the study and manipulation of macromaterials in many disciplines of science and technology demands improved separation tools with greater range, resolution, and versatility. The FFF process fulfills many of these needs by providing high selectivity and speed, simultaneous measurement, simplified coupling to other measurement devices, automation, ready fraction collection, applicability to diverse samples over a broad mass-size range, gentleness in separating delicate species, and flexibility in targeting specific problem areas. In addition, FFF is intrinsically simple and theoretically tractable. As a result, theory provides many useful guidelines for experiment and it underlies a broad capability for measurement (see below).

The FFF process was first conceptualized in the 1960s (*11*); accounts of the invention and subsequent work have been published (*6, 12, 13*). A couple of decades were required to gain a working base of FFF subtechniques (*13*) and to adapt instrumentation and procedures to experimental needs. Three recent international symposia on FFF (*14*) have highlighted the many important applications that are rapidly emerging (see below).

Although FFF is still at an early stage of development, the ensemble of techniques and applications are already remarkably diverse. Inherent diversity is a long-term strength of FFF. Unfortunately, diversity has so diluted focus that FFF is not now utilized for many promising applications because experimental precedence and protocols are lacking. Examples given below are suggestive of new possibilities.

Mechanism of FFF

The FFF mechanism combines elements of chromatography and field-driven techniques such as electrophoresis and ultracentrifugation (*1–10, 15*). Like chromatography, FFF is an elution technique with un-

The author is with the Field-Flow Fractionation Research Center, Department of Chemistry, University of Utah, Salt Lake City, UT 84112.

derlying roots in differential flow displacement; like field-driven techniques, FFF requires a field or gradient.

The field in FFF acts unconventionally; it does *not* directly drive separation. Instead, the field is applied at right angles to flow and serves to drive components into different stream laminae in a thin (50- to 300-μm) channel. The unequal velocities of the laminae then cause the separation, which unfolds along the flow axis. The perpendicular orientation of field and separation axes clearly distinguishes FFF from traditional field-driven methods.

The FFF mechanism is illustrated in Fig. 1. Here the component bands X and Y are separated by flow in a thin ribbonlike channel, the preferred channel geometry for FFF. The flow profile in the channel (except near the edges) is parabolic, like that between infinite parallel plates. The channel flow propels X and Y toward the outlet. However, the displacement velocities of X and Y depend on the mean positions of the bands in the parabolic profile. These positions are controlled by the right-angle field.

The field used in FFF must be strong enough to drive the components of interest into localized laminae (preferably <10 μm thick) within the parabolic profile. Usually the components are driven into equilibrium distributions close to one wall, termed the accumulation wall. Those components (such as Y) forming distributions closest to the accumulation wall are entrained in the slowest flow laminae and are thus displaced downstream most sluggishly. They gradually separate from more highly elevated components (such as X) positioned in faster laminae.

From within the general mechanistic framework described above, several specific (and often quite divergent) separation mechanisms arise. These mechanisms differ depending on factors controlling particle distributions: Diffusion, steric effects, hydrodynamic lift forces, density and pH gradients, wall interactions, secondary partitioning, and cyclical-field transport (*6*, *10*, *16*). Most polymers and submicrometer particles are separated by the normal mechanism described below ("normal" because it is the oldest and most widely used mechanism). Use of this mechanism is termed normal mode operation.

Consider two polymer or particle (hereafter particle) populations (such as X and Y) in an FFF channel. The field drives the two particle clouds toward the accumulation wall. The concentration gradient set up by field-driven motion is opposed by diffusion. When these two transport processes balance, particle concentration c (relative to wall concentration c_0) approaches an exponential function of elevation x above the accumulation wall (*10*, *16*, *17*):

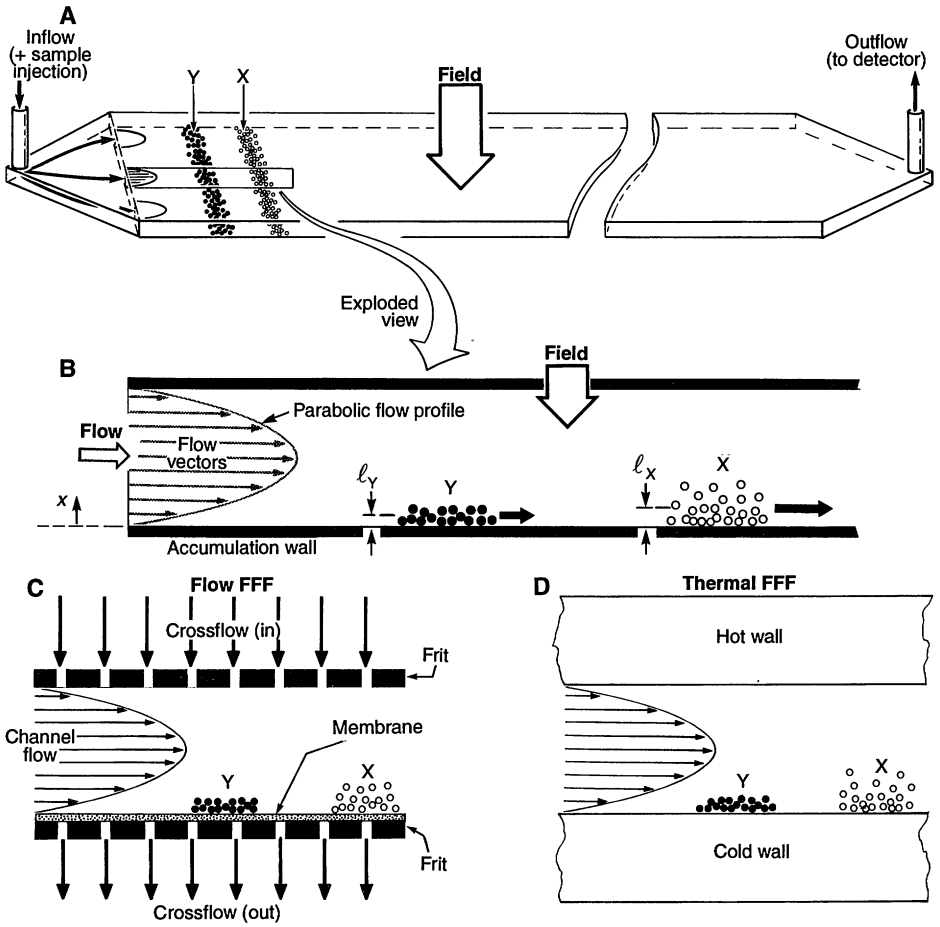

Fig. 1. Elements of FFF separation. (**A**) The ribbonlike FFF channel is usually constructed by cutting the channel volume from a thin spacer and sandwiching between appropriate walls. The thickness of the channel is usually 75 to 260 μm. Channel breadth is a few centimeters and length is some tens of centimeters. Any sensitive detector can be used at exit, including ultraviolet spectroscopy, light scattering, and so on. (**B**) The exploded view shows the different distributions of two arbitrary components X and Y across the parabolic flow profile and the unequal flow displacement velocities that result. For normal mode operation, the X and Y clouds are distributed exponentially above the accumulation wall with characteristic (mean) elevations ℓ_X and ℓ_Y. Two important FFF techniques: (**C**) flow FFF and (**D**) thermal FFF. Separation in flow FFF is driven by a "crossflow" field and in thermal FFF by a temperature gradient.

$$c = c_0 \exp(-x/\ell) \quad (1)$$

where ℓ is the characteristic elevation of the particle cloud. Separation occurs if the ℓ's differ. The ℓ for each component is the ratio of diffusion coefficient D and field-induced velocity U:

$$\ell = D/|U| \quad (2)$$

More insightful is the relation of ℓ to the force F exerted by the field on a single particle (*10*, *18*):

$$\ell = kT/|F| \quad (3)$$

where k is Boltzmann's constant and T is absolute temperature. This equation shows that F controls ℓ and thus governs separation. Values of ℓ can be controlled to achieve optimal levels (usually 1 to 10 μm) by varying the field strength, which changes F proportionally.

The so-called standard model for normal mode retention assumes that all particles are noninteracting point masses. The velocity $\mathcal{V}$ of a cloud of such particles is simply the average velocity of an exponential distribution embedded in a parabolic flow profile. Retention time $t_r = L/\mathcal{V}$, where L is channel length; thus (*10*):

$$\frac{t_r}{t^0} = \frac{w}{6\ell}\left[\coth\frac{w}{2\ell} - \frac{2\ell}{w}\right]^{-1} \quad (4)$$

When ℓ is written in terms of F using Eq. 3, then:

$$\frac{t_r}{t^0} = \frac{|F|w}{6kT}\left(\coth\frac{|F|w}{2kT} - \frac{2kT}{|F|w}\right)^{-1} \quad (5)$$

where t^0 is the void time (the emergence time of a nonretained tracer) and w is channel thickness. When $w >> \ell$, as it should be for efficient operation, the term in brackets approaches unity and t_r/t^0 is approximated by:

$$\frac{t_r}{t^0} = \frac{w}{6\ell} = \frac{|F|w}{6kT} \quad (6)$$

Thus t_r is roughly proportional to F. The separation of particle bands X and Y (Fig. 1), represented by the finite increment Δt_r in their retention times, is achieved only if the force increment ΔF between them is sufficient; only $\sim 10^{-16}$ N is required.

Force (and t_r) usually increase with particle diameter d (or molecular weight M). Most often $F \propto d^n$ with $n = 1$ to 3. A large n implies high selectivity: a rapid change in t_r with d. Specifically, size selectivity (*19*) is defined as $S_d = |d \log t_r / d \log d|$; thus $S_d \cong n$.

The magnitude of F and ΔF depend on particle properties, field strength, and type of field (*8*, *10*). Prominent FFF fields are based on sedimentation (giving sedimentation FFF), crossflow (flow FFF), temperature gradients (thermal FFF), and electrical fields (electrical FFF).

The FFF Family

The above fields (and others) can be combined in many ways with the different FFF mechanisms to spawn a sizable family of FFF techniques (*6*, *10*, *16*). A simplified core of techniques is described below.

Sedimentation FFF. Here the channel encircles the centrifuge axis like a belt (*20*) (Fig. 2). The spinning of the channel generates differential acceleration forces at right angles to flow. These forces are highly selective in separating colloidal and larger particles.

The single-particle force in sedimentation FFF can be written in several forms:

$$|F| = m'G = V_p|\Delta\rho|G = \frac{\pi}{6} d^3|\Delta\rho|G \quad (7)$$

which shows the proportionality of F to effective mass (true mass less buoyant mass) m', particle volume V_p, the cube of diameter (or, for nonspheres, effective spherical diameter) d, the difference $\Delta\rho$ in density between the particle and carrier liquid (*21*), and, of course, field strength or acceleration G. Thus colloidal particles can be separated (see Eq. 5) based on differences in m', V_p, d, or $\Delta\rho$, with the separation modulated by the spin rate used to control G.

A sedimentation FFF apparatus designed at the Field-Flow Fractionation Research Center (FFFRC) is shown in Fig. 2A. The separation of several sizes of polystyrene (PS) latex beads at two different spin rates in this device is shown in Fig. 2C. As predicted (Eqs. 6 and 7), t_r increases with both d and G.

The rough proportionality of t_r to d^3 explains why particles differing only slightly (down to 5 to 10%) in size can be separated. In some respects, the size selectivity ($S_d \cong 3$) is too great. A fivefold size difference elutes over a t_r range of ~125-fold, making t_r excessively long for larger ds. The long separation time is unacceptable. It is remedied by programming the field strength downward so that late-eluting particles are hastened out of the channel (*22*) (Fig. 2D). Resolution is most uniform when G is reduced with time according to a special power program (*23*). (When programming is used, Eqs. 4 to 6 are no longer valid.)

Sedimentation FFF and ultracentrifugation differ in many respects other than mechanism. The displacement rate of particle bands depends on different factors: F alone in sedimentation FFF and F/f (where f = friction coefficient) in ultracentrifugation. (Particle shape as well as mass governs F/f, which can complicate interpretation.) FFF is more flexible in operation than ultracentrifugation; field strength and flow rate can be manipulated to attain speed and resolution targets. Although FFF, as an elution technique, provides direct fraction collection and on-line coupling with other measuring instruments, elution requires rotating seals to continuously transfer carrier liquid to and from the FFF channels. These seals are troublesome at high spin rates, although Kirkland *et al.* have demonstrated feasibility up to $\sim 10^5 g$ (*24*). Because of seal and other limitations, sedimentation FFF is difficult to apply to particles smaller than 10 to 30 nm in size (depending on density and maximum field strength) and polymers $<10^6$ to 10^7 daltons. Other FFF techniques are advantageous for separating smaller species.

Flow FFF. Flow FFF is more universally applicable than sedimentation FFF. It is capable of separating almost all particles and polymers down to ~1 nm in size (*25*). In flow FFF, two right-angle flow streams

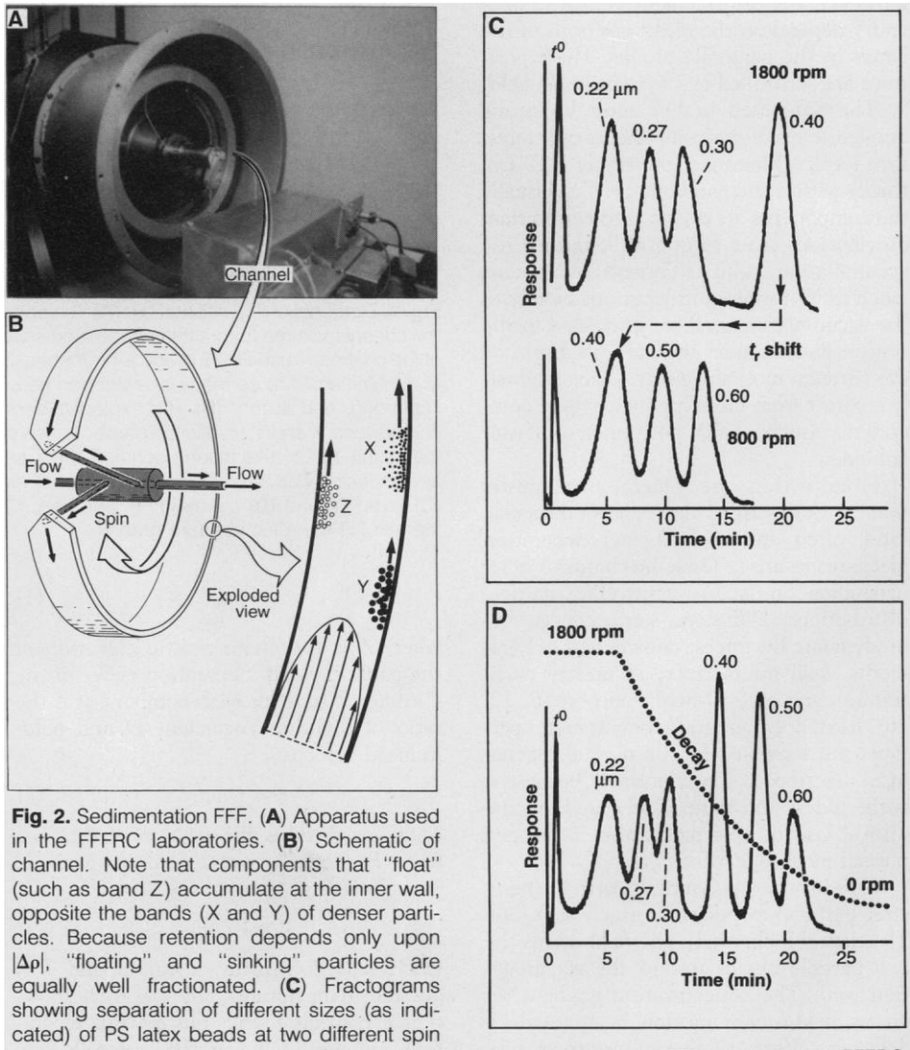

Fig. 2. Sedimentation FFF. (**A**) Apparatus used in the FFFRC laboratories. (**B**) Schematic of channel. Note that components that "float" (such as band Z) accumulate at the inner wall, opposite the bands (X and Y) of denser particles. Because retention depends only upon $|\Delta\rho|$, "floating" and "sinking" particles are equally well fractionated. (**C**) Fractograms showing separation of different sizes (as indicated) of PS latex beads at two different spin rates; the ability to shift retention by changing field strength is shown. [FFF runs by Y. Xu, FFFRC. Flow rate = 2.5 ml/min and w = 127 μm.] (**D**) Programmed field run showing how a wider diameter range can be condensed into a reasonable elution span by reducing the rotation rate (as shown). Here the field strength is decayed according to power programmed operation. [Conditions, except for rotation rate, are the same as for (*C*).]

are superimposed (Fig. 1C). The channel stream sweeps components toward the outlet. The crossflow stream, entering and exiting through permeable walls (*26*), drives components toward the accumulation wall—a membrane layered over a frit. The pore size of the membrane determines the lower size limit for separation.

The driving force in flow FFF is the viscous force exerted on a particle by the crossflow stream. Stokes law gives (*25*):

$$|F| = f|U| = 3\pi\eta|U|d = kT|U|/D \quad (8)$$

where the final term arises from the Stokes-Einstein relation, $D = kT/f$. Here d is the Stokes (or hydrodynamic) diameter of the particle, η is viscosity, and U is the crossflow velocity. Combination with Eq. 6 shows that t_r is proportional to f, d, and D^{-1}.

The apparatus for flow FFF, which does not require a centrifuge, is simpler than that for sedimentation FFF (*27*). It not only reaches to smaller particle sizes but it separates all particles, even neutrally buoyant ones, independently of density. Interpretation is simple because separation is based on size alone, with t_r approximately proportional to diameter. This first-power dependence ($S_d = 1$) means that t_r is less sensitive to diameter than in sedimentation FFF ($S_d = 3$). Nonetheless, selectivity is still relatively high, well exceeding that of size exclusion chromatography or SEC ($S_d \approx 0.2$). Because S_d is lower for flow FFF than sedimentation FFF, the t_r range is more condensed and programmed field operation is usually unnecessary.

Flow FFF is flexible in channel design. A hollow fiber can serve as the channel (*28*). An asymmetrical channel having one nonpermeable wall is a highly successful variant (*29–31*).

Thermal FFF. Thermal FFF evolved as a technique for separating synthetic polymers in organic solvents (*32*). More recently, both aqueous and nonaqueous particle suspensions, along with mixtures of polymers and particles, have been shown to be separable (*33*).

Thermal FFF is driven by a temperature gradient (Fig. 1D). The ribbonlike channel is sandwiched between high heat-conductivity (metal) blocks that can supply and remove sufficient heat to maintain gradients (dT/dx) of $\sim 10^4$ K per centimeter (for example, a temperature drop $\Delta T \approx 10^2$ K over a distance $w \approx 10^{-2}$ cm). Polymers and particles are generally driven toward the cold wall by thermal diffusion (*34, 35*). The effective driving force per polymer molecule is:

$$|F| = kT\frac{D_T}{D}\frac{dT}{dx} \quad (9)$$

where D_T is the coefficient of thermal diffusion. For polymers with $D \cong AM^{-b}$ ($b \approx 0.6$), the dependence of t_r on molecular weight M is found by combining Eqs. 9 and 6 (*36*):

$$\frac{t_r}{t^0} \cong (D_T/A)\Delta T M^b \quad (10)$$

in which ΔT has replaced wdT/dx. The prediction that t_r increases with M is borne out by experiment (see Fig. 3A).

Unlike the predictable retention of sedimentation and flow FFF, retention in thermal FFF is made uncertain by D_T, which cannot be calculated. This difficulty is partially remedied by thermal FFF itself, which has provided abundant D_T measurements (see below).

Electrical FFF. In principle, the high intensity and manipulability (such as through pH changes) of electrical forces should have carved a major niche for electrical FFF (*37, 38*). Instead, problems in handling electrolysis gases have made electrical FFF an orphan in the FFF family. Only recently has this status begun to change, particularly with the work of Caldwell and Gao (*39*).

Electrical driving forces are proportional to net charge q. Separation is thus based on charge differences Δq. In the more familiar case of electrophoresis, separation is based on differences in electrophoretic mobility, which is proportional to $\Delta(q/f)$ (*38*).

Steric FFF. Unlike the preceding categories of FFF, steric FFF invokes a new mechanism, not a new field. It is a mechanism applicable to larger particles (~0.5 to 200 μm). Here forces are larger and diffusion, which is strongly suppressed, no longer plays a major role in retention (*40, 41*).

Consider a sphere of diameter d (for example, 10 μm) driven toward the accumulation wall by field forces. Motion is halted by the physical (steric) barrier of the wall when the particle center approaches distance $x = d/2$ above the wall. Thus the equilibrium elevation of the particle depends upon its size. Larger particles, more highly elevated than their smaller counterparts, are swept downstream more rapidly. Thus large particles elute before small particles, a trend opposite to that found for the normal mode of FFF.

The mechanism of steric FFF is complicated by hydrodynamic phenomena (*41*). Foremost are hydrodynamic lift forces that tend to drive particles away from the wall (*42–44*). Two choices exist. The driving forces can either be increased sufficiently to offset lift forces and confine the particles close to the wall, or they can be adjusted to allow the particles to gain a significant elevation above the wall, where they form hyperlayers. The former corresponds to the steric mechanism and the latter to a related FFF mechanism, that of lift-hyperlayer FFF (see below).

Steric FFF has been most successfully implemented (with $S_d \approx 0.8$) by using sedimentation forces (sedimentation-steric FFF). Whereas gravitational forces were first used to separate micrometer-sized particles (*40*), high-speed separation requires the use of a centrifuge to offset lift forces.

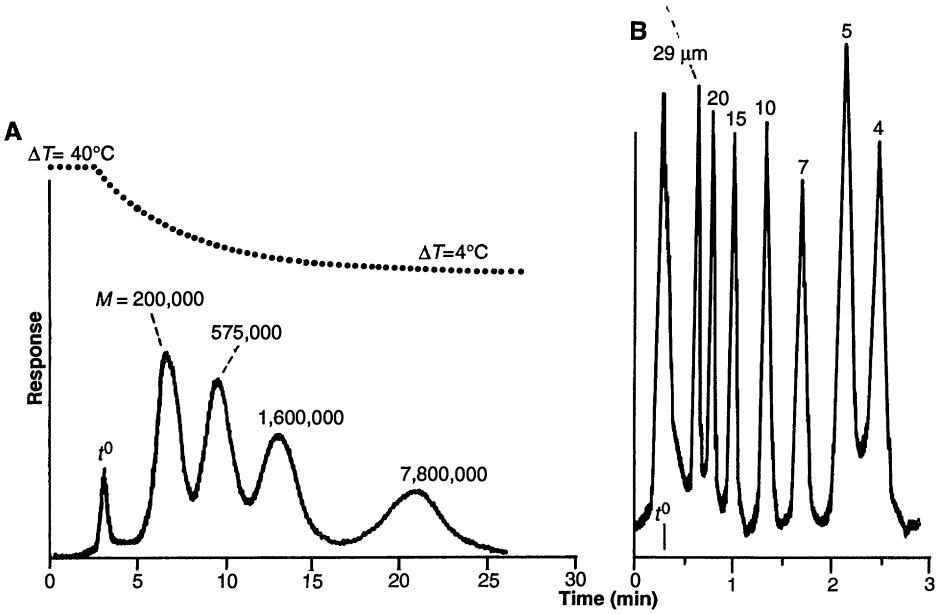

Fig. 3. Separation of unlike macromaterials by different FFF techniques. (**A**) Separation of high molecular weight linear PS polymers in tetrahydrofuran (THF) by power programmed thermal FFF. [From P. Chen, FFFRC. Flow rate = 0.2 ml/min, and w = 76 μm.] (**B**) High-speed separation of PS latex spheres of seven different diameters by sedimentation FFF operating in steric mode. [M. Moon, FFFRC. Rotation rate held constant at 1325 rpm, flow rate = 6 ml/min, and w = 127 μm.]

Such a separation (Fig. 3B) cleanly revolves seven latex diameters in <3 min.

Lift-hyperlayer FFF. In this mode, selectivity is greatest when F has the weakest dependence upon d; thus crossflow forces are preferable to sedimentation forces (*45*). The resulting subtechnique, flow-hyperlayer FFF, displays high selectivity ($S_d \sim$ 1.2 to 1.5), flexibility, and speed in the separation of micrometer-sized particles. The particles are held well away from the wall during separation and thus beyond the reach of particle-wall disturbances.

FFF as a Measurement Technique

Retention in FFF is governed by field-induced forces. Retention measurements can be converted into numerical values of forces by using established retention relations. Extremely delicate forces can be measured (see below). Also, because many types of forces are involved in FFF, a variety of forces can be measured (6).

Measuring forces on particles can serve two purposes. One is to measure particle properties. For fields (such as sedimentation and crossflow) with well-understood force laws, forces depend in a calculable way on particle mass, size, density, charge, diffusivity, thickness of adsorbed layers, shell structures, and, indirectly, composition. These and other properties can be obtained through FFF retention measurements (Eqs. 5 and 6). The value of this measurement capability is enhanced by the fractionating power of FFF: species can be subjected to measurement even as they are isolated from complex matrices. Thus the properties of multiple intermixed components can be measured in a single run. For populations with a continuum of properties, the property distribution can be measured, yielding mass distribution, size distribution, and so on.

The measurement of forces serves a second purpose: contributing to the understanding of physicochemical phenomena. For example, for ill-defined force laws (lift forces) or transport phenomena (thermal diffusion), the measurement of forces exerted on particles having known properties can help clarify the governing laws.

For colloids and macromolecules subject to normal-mode FFF, retention is induced by minute forces—from 10^{-16} to 10^{-14} N per particle (6). Thus forces as small as 10^{-16} N can be determined by measuring t_r. Increments in forces as low as 10^{-17} N can be detected as measurable shifts in t_r of 0.1 to 1 min (*46*). These forces are eight to nine orders of magnitude less than the force [0.8×10^{-8} N (*47*)] required to rupture one C–C bond. The small magnitude of observable forces is a result of their being balanced against the weak entropy-based forces driving the expansion of the Brownian particle cloud. For micrometer-sized particles subject to steric or lift-hyperlayer FFF, driving forces, balanced against lift forces, tend to be higher, 10^{-14} to 10^{-8} N per particle.

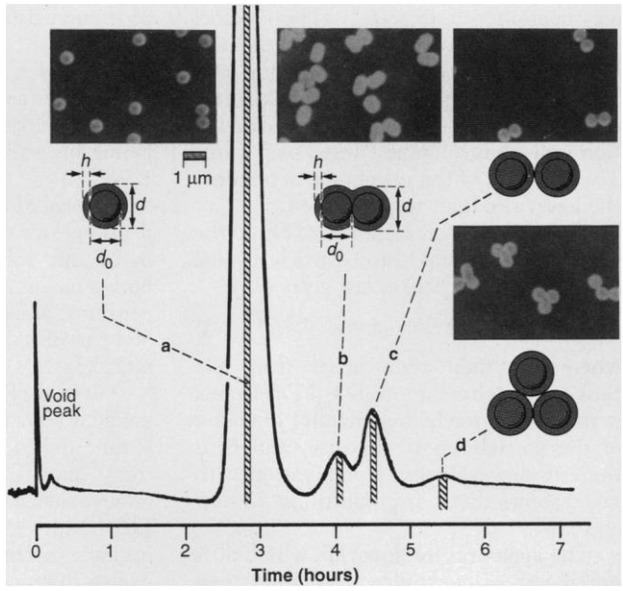

Fig. 4. Separation of components of partially aggregated PMMA latex by sedimentation FFF (*51*). Singlets are isolated from doublet and triplet clusters and examined by EM, giving the results shown in the micrographs. The surprising observation of two doublet peaks, the first occupied by tightly fused doublets of lesser mass, is consistent with a two-stage latex growth and aggregation process (see text). A low flow rate (0.38 ml/min) and long retention times were utilized in order to maximize resolution of the doublets. [Adapted from (*51*) with permission © American Chemical Society]

Sedimentation FFF. Sedimentation forces are given by Eq. 7. Retention (force) measurements are seen to give effective mass m' directly. If particle density is known, particle mass m, volume V_p, and effective spherical diameter d can be calculated (*48*, *49*). Because of separation, m', m, V_p, and d distribution curves can be measured (*50*).

The measurement of mass and mass distribution can help dissect many colloidal phenomena, including aggregation (*51*). The fractogram for a partially aggregated polymethylmethacrylate (PMMA) latex is shown in Fig. 4. Singlet, doublet, and triplet particle clusters are cleanly resolved. For singlet (single-sphere) retention, the calculated value of d is 0.54 μm, in agreement with electron microscopy (EM). Remarkably, there are two doublet peaks that differ by ~10% in t_r. This implies two doublet populations differing 10% in mass. The two peaks suggest a two-stage latex growth process, the lighter doublets forming after first-stage growth and the heavier doublets after the second stage. Back calculations yield a first-stage d_0 = 0.30 μm, with thickness h = 0.12 μm added in the second stage (see Fig. 4). The lighter doublets should thus be shortened from 1.08 μm to 2(0.30 + 0.12) μm = 0.84 μm. They should be highly fused. These observations are confirmed by EM (see Fig. 4), an invaluable adjunct tool.

For most colloids, particle density ρ_p is known. If ρ_p is not known, the measured force is associated with two unknowns: d and $\Delta\rho$ or equivalently m and ρ_p. This uncertainty is resolved by measuring retention at two or more carrier liquid densities ρ (*52*). A plot of ρ versus m' yields a straight line whose intercept on the ρ axis is ρ_p and on the m' axis is m. All of the above particle parameters are then specified. Measurements made close to the point of neutral buoyancy yield ρ_p to four-figure accuracy. Carrier densities far removed from neutral buoyancy provide ρ_p by extrapolation. This approach, used for viruses (*53*, *54*), yields ρ_p without exposing fragile particles to highly modified dense media.

Various strategies can be used to characterize complex particles. For example, for multiphase particles $m' = \Sigma m_i'$, where m_i' is the effective mass of phase i (*55*). Such particles include core-shell latexes and liposomes. For these two-phase shelled structures, m' = m'(shell) + m'(core). If the carrier density is adjusted to make the core neutrally buoyant, m'(shell) (and its distribution) is obtained from retention measurements. For liposomes, where the shell is a uniform phospholipid bilayer, m'(shell) gives a measure of shell area A. For unilammelar vesicles, $A \propto d^2$. Conversely, if m'(shell) is negligible because of shell thinness or near neutral buoyancy, m'(core) is measured. Depending on circumstances, m'(core) may specify core volume or, for liposomes, drug loading (*55*).

Related measurements provide the mass or thickness of adsorbed layers on particles (*56*, *57*). Before adsorption, m' = m'(particle). After adsorption, the measured gain $\Delta m'$ = m'(layer). Equations 6 and 7 give:

$$\Delta m' = (6kT/Gw)\Delta t_r/t^0 \qquad (11)$$

We calculate that $\sim 10^{-17}$ g of adsorbed mass (density 1.4 g/cm^3) can be discerned by a retention time shift $\Delta t_r = 0.3t^0$ at a modest G ($10^3 g$) when $w = 250$ μm. This mass corresponds to a layer ~0.6 Å thick on a 0.2-μm sphere (*57*).

The above approach has been used to measure protein adsorbed on latex surfaces (*57–59*), which is relevant to immunodiagnostic assays and biomedical implants. Complete adsorption isotherms can be measured (*57*) and antigen-antibody binding ratios determined (*58*). Whereas sedimentation FFF provides a direct measure of adsorbed mass increments, competing techniques are indirect or suffer other uncertainties (*58*).

Flow FFF. The measurement of retention in flow FFF directly yields Stokes diameter d, friction coefficient f, and diffusion coefficient D, as seen by combining Eq. 8 with Eqs. 5 or 6. There is no interference by (or opportunity to measure) density, which does not affect retention.

The diffusion coefficients of proteins and latex beads were measured in early studies on flow FFF and found in good agreement with previously reported values (*60*). More exhaustive measurements were recently made on double- and single-stranded DNA (*61*) and on proteins (*62*). Accuracy appears better than 5% and is comparable to other techniques. The measurement is rapid (usually 1 to 10 min) and simple. Diffusivities can be directly measured for minor constituents (like protein aggregates) that cannot be sufficiently isolated for traditional measurements.

Retention can be used to measure the size of monodisperse colloids or the size spectrum or distribution of polydisperse colloids (*25*). Because size selectivity is high ($S_d = 1$), shifts in size of only a few percent can be discerned. Ratanathanawongs in this laboratory has been able to track the pH-sensitive thickness of an acrylate shell on a core-shell latex (*63*).

Thermal FFF. The measurement of t_r and F directly yields the Soret coefficient D_T/D (see Eq. 10). If D is known, D_T can be obtained. However, few scientists care to know D_T for their polymers or particles. If D_T were related to mass or composition, its measurement would be valuable. Unfortunately, no valid relation is known (*64*). In this regard, the measurement of D_T creates a bank of D_T data to guide theoretical modeling and generates empirical relationships to convert retention measurements into polymer (or particle) molecular weight and composition.

Thermal FFF is a convenient technique for measuring thermal diffusion parameters (*65*), and a large database has accrued. For polymers, D_T is found virtually independent of chain length and chain branching. It is strongly dependent on polymer and solvent composition (*64*). For random copolymers, D_T varies linearly with monomer percentage; block copolymers display more complex behavior (*66*). For particles, D_T appears to be both composition and size dependent (*33*).

The two factors (D and D_T) controlling polymer retention are opposites: D depends only on physical polymer dimensions, and D_T depends solely on chemical composition. Thermal FFF has been used mainly to discriminate between chain length differences (reflected in D) within polymer families, yielding molecular weight distributions (MWDs) (*67, 68*). The promise of compositional differentiation and measurement based on D_T has been little exploited.

Steric FFF. Steric and lift-hyperlayer FFF provide powerful means for mapping out hydrodynamic lift forces (*41*). Retention times are measured for well-characterized particles such as latex spheres under widely varying conditions. Each t_r value specifies particle velocity and thus position (after correcting for slip) in the parabolic profile. The calculable driving force is equal and opposite to the lift force F_L; thus F_L is known. F_L is examined as a function of particle diameter d, shear rate at the wall s_0, and elevation above the wall δ. Our results verify inertial lift force theories (*42–44*) but suggest the existence of an additional near-wall lift force: $F_L \propto s_0 d^3 \eta/\delta$. The origin of this incremental force is unclear but may relate to lubrication phenomena.

Steric FFF, when used as described above, is a prolific source of high-precision force data for the study of particle hydrodynamics near walls. (The data are obtained from measured peak positions in high-speed fractograms like that in Fig. 3B.) With calibration, particle diameters and densities can also be measured (*69*).

Other measurement strategies. Many other possibilities exist for measurement by FFF. The use of other fields (electrical, dielectrical, magnetic, and so forth) will yield additional parameters. Band broadening measurements can complement retention data (*12, 49*). Coupling FFF and other techniques can enhance measurement capabilities; the use of photon correlation spectroscopy, for example, to determine the size of spheres eluted at time t_r from sedimentation FFF yields both size and density (*70*). The coupling of one FFF instrument to another opens the possibility of obtaining two-dimensional distributions to better define complex materials: Sedimentation and flow FFF should provide the size-density distribution of complex colloids, whereas thermal and flow FFF would yield the composition–molecular weight distribution of copolymers.

Biological and Biomedical Applications

Although FFF is not well known in most fields related to biology, enough applications have emerged in a few key areas to suggest its broader potential. These applications span a billionfold mass range from small proteins to cells and 70-μm starch granules. Between these extremes, FFF has been applied to protein aggregates and conjugates, protein particles, lipoproteins, viruses, DNA, subcellular particles, milk colloids, cell lysates, polysaccharides, liposomes, pharmaceutical emulsions, chromosomes, bacterial cells, and pollen grains, among others.

Biopolymers. Proteins have long been recognized as separable based on charge differences by electrical FFF (*37*) or on size differences by flow FFF (*71*). While the early electrical FFF work was not followed up, flow FFF now separates proteins that differ by 15 to 30% in Stokes diameter in 3 to 10 min. Resolution falls short of theory, suggesting that further gains are possible.

A more difficult problem that can be tackled with flow FFF is the separation of protein complexes. Protein dimers (Fig. 5A) elute as satellite peaks at $\sim 1.4t_r$(monomer). Wahlund's group has found up to four satellite peaks for increasing sizes of monoclonal antibody aggregates (*72*) (Fig. 5B). My group has probed the distribution of Stokes diameters for conjugates of proteins and synthetic polymers. Detailed size distributions are readily obtained in all cases.

DNA has been separated by both sedimentation FFF (*73*) and flow FFF (*29, 30, 61*) (Fig. 5). Microgram quantities can be separated and purified in 5 to 15 min (*61*). Proteoglycans have been fractionated by sedimentation FFF (*74*). Dextrans, Ficolls, pullulans, and the starch polymers amylose and amylopectin have been separated by thermal FFF (*75*).

Bioparticles. Viruses are among the first bioparticles studied by FFF (*48, 76–78*). Viruses can be separated from other viral types or from macromolecular and particulate contaminants by both sedimentation FFF and flow FFF. Viral aggregates (singlets, doublets, and so forth) of the gypsy moth nuclear polyhedrosis virus were readily separated by sedimentation FFF (*77*). The molecular weights, sizes, and densities of viral particles have been measured (*48, 54, 76–78*). Collected fractions retain infectivity, demonstrating the gentleness of the process (*77, 78*).

Mozersky, Caldwell, and co-workers have used sedimentation FFF (coupled to subsequent assays) to analyze subcellular particles including mitochondria and microsomes (*79*). Sedimentation FFF has also been used to characterize protein particles

including those responsible for optical clouding in cataractous human lens (*80*). It has been coupled to gas chromatography–mass spectrometry (GC-MS) to characterize cell wall particles (*81*) and used for the size determination of the Creutzfeldt-Jakob disease agent (*82*). High, low, and very low density lipoproteins (which differ in size as well as density) are separable by flow FFF (Fig. 5C). Metaphase chromosomes (up to 8 μm long) have been partially fractionated by steric FFF.

Liposomes and emulsions. Pharmaceutical colloids, including liposomes and emulsions, are subject to fractionation by FFF. Size distributions and densities (where necessary) can be determined. The first (*83, 84*) and most subsequent studies (*70, 85, 86*) were done by sedimentation FFF. However, size distribution measurements are more straightforward by flow FFF (*55*).

Cells. Steric FFF is a promising technique to separate cells >2 μm in diameter because of its high speed and convenient operation (*87*). Applicability to mammalian cells (HeLa + various erythrocytes) was shown in 1984 (*88*). Recently, a suite of new capabilities emerged. Cardot, Martin, and co-workers have shown that abnormal blood cells (from anemia or transfusions) can be distinguished from healthy erythrocytes in a simple 1g FFF channel (*89, 90*). Also, a prevalent parasite (microfilariae) can be isolated from blood, suggesting rapid diagnosis (*91*). Bigelow *et al.* have separated B and T lymphocytes, although physically indistinguishable, using FFF channels with selective wall adhesion (*92*). Barman and co-workers have used flow FFF (in the lift-hyperlayer mode) for the high-speed (2 to 3 min) fractionation of normal and abnormal erythrocytes from various species (*87, 93*) (see Fig. 6A). Biotechnology relevance was shown by Hoffstetter-Kuhn and co-workers who determined the growth and cell cycle distribution of yeast cells in cultivation broths by sedimentation-steric FFF (*94*).

Alternate FFF mechanisms are applicable to some cells. Normal-mode FFF readily fractionates small unicellular organisms (next section). *Escherichia coli* can be separated based on motility differences because high motility is equivalent to a large diffusivity (*D*) in Eq. 2 (see Fig. 6B).

Industrial and Environmental Applications

An enormous variety of large and small particles and polymers are major components of industrial products or are used in synthesizing and processing these products. Product quality is profoundly affected by size, mass, and compositional distributions of these macromaterials. With increasing industrial emphasis on quality control, FFF is gaining relevance as a useful tool to dissect materials and measure constituent properties.

Industrial colloids and particles. Sedimentation FFF has been used to fractionate and determine the size distribution of numerous industrial colloids, including carbon black, silica particles, pigments, metal and ceramic particles, clay, and a host of latexes (*95*). Flow FFF has been applied to similar colloids with some emphasis on nanoparticles (such as colloidal silica and seed latex) down to 2 nm in size (*25*).

Larger industrial particles (>0.3 to 1 μm) are rapidly fractionated and characterized by sedimentation-steric FFF. Gold, palladium, silver, and copper particles in the size range from 0.3 to 15 μm were separated

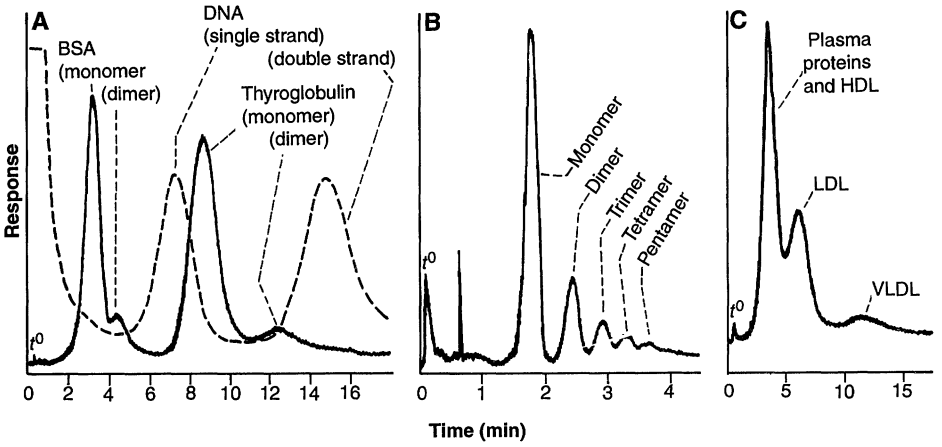

Fig. 5. Separation of biopolymers and bioparticles by flow FFF. (**A**) Separation of two proteins (bovine serum albumin and thyroglobulin) and their aggregates (solid line). Separation of single- and double-stranded DNA of equal contour length (5386 bases or base pairs). [FFF of proteins by P. Li, FFFRC, and FFF of DNA by M.-K. Liu, FFFRC.] (**B**) Separation of monoclonal antibody from its aggregates, showing separable peaks up to aggregation number 5 (pentamers). [Results, from asymmetrical flow FFF, courtesy of K.-G. Wahlund, University of Lund, Sweden (*72*).]. (**C**) Fractionation of very low, low, and high density lipoprotein components (VLDL, LDL, and HDL, respectively) from blood plasma. High density lipoprotein particles are in the same size range as larger plasma proteins (such as γ-globulin), causing an overlap of the two; smaller proteins have been eluted through the membrane. [Work done by P. Li, FFFRC.]

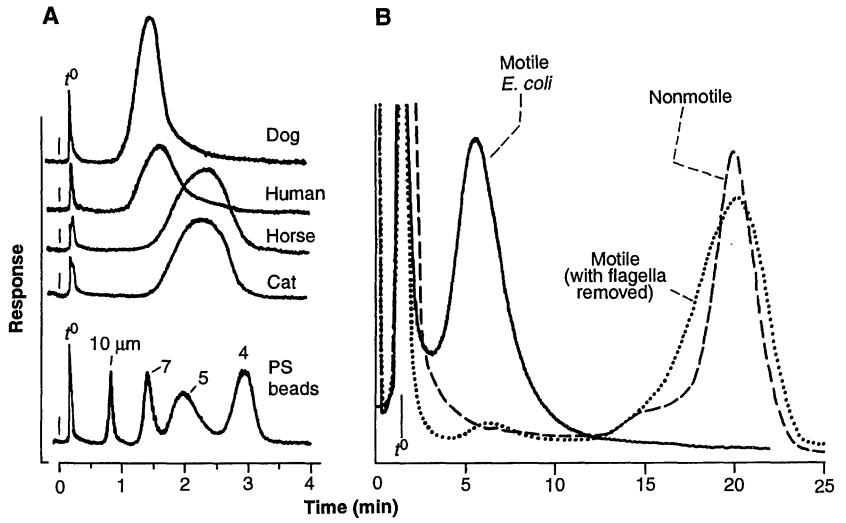

Fig. 6. Application of FFF to biological cells. (**A**) Rapid fractionation of different mammalian red blood cells by flow-hyperlayer FFF (*87*). [Reprinted from (*87*) with permission © American Chemical Society] Relative sizes are established by the fractogram of PS latex beads of known diameters shown at the bottom. The cell peaks are relatively wide because of size polydispersity. (**B**) Separation of *Escherichia coli* cells by sedimentation FFF. Separation is based on motility differences. The fully motile ("tumbly") cells emerge first because of their high effective diffusivity *D* (see Eqs. 2 and 6). Nonmotile cells (lacking flagella) elute later. Their t_r is virtually identical to that observed for motile cells whose flagella have been sheared off. [Work done by Y. Jiang, FFFRC; *E. coli* strains courtesy of J. S. Parkinson, Biology Department, University of Utah. Conditions: spin rate = 200 rpm, flow rate = 2.8 ml/min, and w = 254 μm.]

and their size distributions determined in less than 12 min (96). Larger particles are processed faster; 3- to 15-μm copper particles required only 60 s. In other studies, 2- to 70-μm starch granules, 7- to 65-μm polyvinylchloride latex (97), 3- to 70-μm alumina (97), and 2- to 12-μm chromatographic silica (69) have been fractionated in times from 1.5 to 5 min. Flow-hyperlayer FFF, usually faster, has been used to size-fractionate ground minerals and chromatographic silica (25).

For particle populations with aggregates or other shape variants, characterization can be extended by EM. One of the gold samples exhibited a bimodal distribution; the EM of collected fractions demonstrated that the larger mode (at ~0.6 μm) consisted almost entirely of aggregates, mainly quadruplets and quintuplets, of 0.3-μm gold spheres (96) (see Fig. 7).

Synthetic polymers. Thermal FFF has been found applicable to virtually every type of lipophilic polymer examined: polystyrene, polyisoprene, polyethylene, several acrylates, and perhaps a dozen others. Calibration, which is required to obtain an MWD, is based on straight-line plots of log (D/D_T) versus log M (67).

Linear polymers in the range M = 10^4 to 10^7 are well suited for thermal FFF analysis using ΔTs ~ 10 to 100 K. Polymers of lower M (~10^3) need an inconveniently high ΔT (~150 K) for retention. Linear chains with M > 10^7 require reduced flow rates, ΔTs, and sample loads. More compact structures—branched, cross-linked, or condensed (particulate)—can be fractionated at much higher M levels, opening up new opportunities. For example, microgels (which tend to clog SEC columns) can be separated from background polymer (see Fig. 8A), promising to simplify a laborious industrial analysis. Although sizable particles (up to 10 μm) are now known to be separable by thermal FFF (33), we have recently developed the capability of simultaneously fractionating polymers and particles so that the major constituents of composites such as acrylonitrile-butadiene-styrene (ABS) rubber can be separated (99) (Fig. 8B).

Flow FFF performs much like thermal FFF, except that retention is not sensitive to polymer composition. Flow FFF is most attractive for water-soluble polymer analysis (100). Stokes diameter or diffusivity distributions emerge directly; MWDs require a relation (such as $D = AM^{-b}$) between M and D.

Environmental materials. Environmental quality is influenced by a myriad of fine particles that occupy water, soil, and air. The environmental effects of these entities are indirect as well as direct: they often act as vehicles that govern the transport and fate of adsorbed pollutants and nutrients (101). FFF is helping to untangle this particulate-chemical "soup." In particular, FFF capabilities for separation and mass-size measurements are encouraging the on-line and off-line coupling of FFF and element- and chemical-specific analyzers to determine the chemical nature of physically differentiated and characterized fractions (102). This work, spearheaded by Beckett, is beginning to reveal significant correlations between the physical and chemical properties of environmental materials.

The fractionation of natural colloids in river water by sedimentation FFF was reported in the 1980s (103, 104). These studies show that different river sources exhibit different size and mineralogy distribution patterns, which could serve as colloidal "fingerprints." The components within fractions were differentiated according to morphology by EM, elemental content by energy-dispersive x-ray analysis, and mineralogy by x-ray diffraction. In more recent work, the on-line coupling of FFF and inductively coupled plasma MS has simplified and improved the sensitivity of measuring element profiles for different particle sizes (105).

To further correlate physical and chemical properties, Beckett *et al.* have devel-

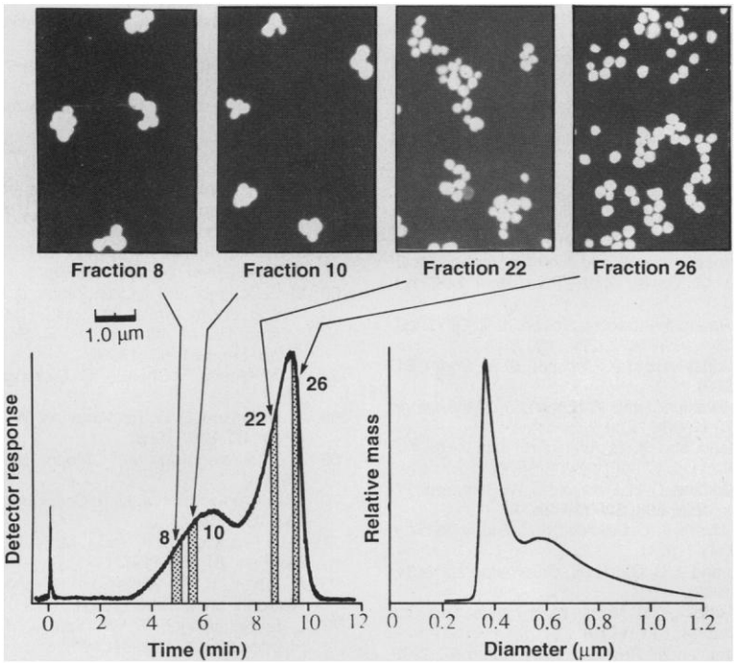

Fig. 7. Fractionation of gold particles by sedimentation-steric FFF. The size distribution (right) is derived from the fractogram at the left based on an empirical calibration plot (96). By coupling EM and FFF, micrographs are obtained which show that the larger size mode consists entirely of aggregates of elementary 0.3-μm gold spheres. [Reprinted from (96) with permission © American Chemical Society]

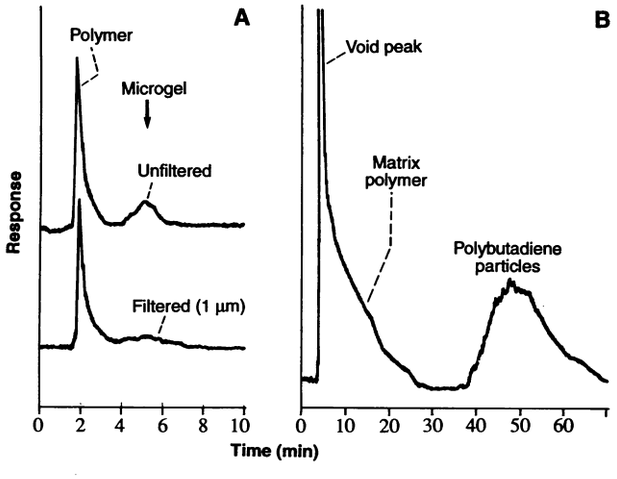

Fig. 8. Separation of components of complex polymeric materials by thermal FFF. (**A**) Isolation of microgel from filtered (1-μm pore size) and unfiltered industrial styrene-butadiene copolymer dissolved in THF. [FFF run by X. Li, FFFRC. Flow rate = 0.36 ml/min, ΔT = 20 *K*, and *w* = 51 μm.] (**B**) Separation of polybutadiene particles from matrix polymer in ABS rubber (99). (Power programmed run with initial ΔT = 90 K, flow rate = 0.185 ml/min, and *w* = 76 μm.)

oped a technique using sedimentation FFF to measure the amount and surface density of adsorbed materials across the particle size range of colloids (*106*). The aim is to understand pollutant transport in rivers and soils. Colloids from soils, for example, are thought to play a major role in the transport of pollutants through soil profiles and ground waters (*107*).

Various FFF methods have shown a distinct advantage over other methods for separating and characterizing soil colloids. By using sedimentation FFF, 20 or more fractions in the size range from 0.1 to 2 μm are generated in 60 to 100 min whereas traditional centrifugation or ultrafiltration procedures take days. Flow FFF has potential for the isolation of organo-mineral complexes (which are found to transport phosphate) in the nanometer size range. There is minimal physical and chemical disruption of the sample, in marked contrast to the chemical and physical extraction methods usually used to remove soil organic components. Again, a major advantage of both flow and sedimentation FFF is that fractions can be collected for both mineralogical identification and chemical analysis (*108*).

Flow FFF is capable of probing into the size niche occupied by humic substances present in natural waters and soils. Although humics play a critical role in many aquatic processes, reliable information on their physical and structural properties has been difficult to obtain. Flow FFF has been used to determine MWDs of humic substances from various environments down to 500 daltons (*109, 110*). This work has been extended to evaluate the effects of various wastewater treatment processes for the removal of organic matter from pulp and paper manufacturing effluents (*111*).

Finally, sedimentation FFF (normal mode) has been used to determine the size, density, and mass of bacterial cells in natural waters. A direct method for estimating bacterial biomass was developed that offers distinct advantages over existing methods used in microbial ecology studies (*112*).

REFERENCES AND NOTES

1. J. C. Giddings, *J. Chromatogr.* **125**, 3 (1976).
2. ———, *Pure Appl. Chem.* **51**, 1459 (1979).
3. J. Janča, *Trends Anal. Chem.* **2**, 278 (1983).
4. R. Beckett, *Environ. Tech. Lett.* **8**, 339 (1987).
5. M. Martin, in *Particle Size Analysis 1985*, P. J. Lloyd, Ed. (Wiley, New York, 1987), pp. 65–85.
6. J. C. Giddings, *Chem. Eng. News* **66** (no. 41), 34 (1988).
7. K. D. Caldwell, *Anal. Chem.* **60**, 959A (1988).
8. J. C. Giddings and K. D. Caldwell, in *Physical Methods of Chemistry*, B. W. Rossiter and J. F. Hamilton, Eds. (Wiley, New York, 1989), vol. 3B, pp. 867–938.
9. S. Levin, *Biomed. Chromatogr.* **5**, 133 (1991).
10. J. C. Giddings, *Unified Separation Science* (Wiley, New York, 1991).
11. ———, *Sep. Sci.* **1**, 123 (1966).
12. ———, *Anal. Chem.* **53**, 1170A (1981).
13. ———, M. N. Myers, K. D. Caldwell, *Sep. Sci. Technol.* **16**, 549 (1981).
14. Reports on the third symposium proceedings have been made by M. Martin [*Anal. Chem.* **65**, 315A (1993)], M. E. Schimpf [*LC-GC* **11**, 46 (1993)], and V. T. Remcho [*Am. Lab. (Shelton)* **1993**, 21 (February 1993)].
15. J. C. Giddings, *J. Chromatogr.* **395**, 19 (1987).
16. M. Martin and P. S. Williams, in *Theoretical Advancement in Chromatography and Related Separation Techniques*, vol. 383 of the *NATO ASI Series C: Mathematical and Physical Sciences*, F. Dondi and G. Guiochon, Eds. (Kluwer, Dordrecht, 1992), pp. 513–580.
17. E. Grushka, K. D. Caldwell, M. N. Myers, J. C. Giddings, *Sep. Purif. Methods* **2**, 127 (1973).
18. With the sign convention that $+x$ is the distance from the accumulation wall, U and F are negative. To avoid unnecessary involvement with sign interpretation, $-F$ and $-U$ are replaced by $|F|$ and $|U|$, respectively.
19. M. N. Myers and J. C. Giddings, *Anal. Chem.* **54**, 2284 (1982).
20. J. C. Giddings, F. J. F. Yang, M. N. Myers, *ibid.* **46**, 1917 (1974).
21. Particle density is assumed equal to the reciprocal of partial specific volume.
22. F. J. F. Yang, M. N. Myers, J. C. Giddings, *Anal. Chem.* **46**, 1924 (1974).
23. P. S. Williams and J. C. Giddings, *ibid.* **59**, 2038 (1987).
24. J. J. Kirkland, C. H. Dilks, Jr., W. W. Yau, *J. Chromatogr.* **255**, 255 (1983).
25. S. K. Ratanathanawongs and J. C. Giddings, *ACS Symp. Ser.* **521**, 13 (1993).
26. The crossflow negligibly disturbs parabolic flow; see J. M. Davis, *Anal. Chim. Acta* **246**, 161 (1991).
27. S. K. Ratanathanawongs, I. Lee, J. C. Giddings, *ACS Symp. Ser.* **472**, 229 (1991).
28. J. Å. Jönsson and A. Carlshaf, *Anal. Chem.* **61**, 11 (1989).
29. K.-G. Wahlund and A. Litzén, *J. Chromatogr.* **461**, 73 (1989).
30. A. Litzén and K.-G. Wahlund, *ibid.* **476**, 413 (1989).
31. J. J. Kirkland, C. H. Dilks, Jr., S. W. Rementer, W. W. Yau, *ibid.* **593**, 339 (1992).
32. M. N. Myers, K. D. Caldwell, J. C. Giddings, *Sep. Sci.* **9**, 47 (1974).
33. G. Liu and J. C. Giddings, *Chromatographia* **34**, 485 (1992).
34. J. C. Giddings, M. Martin, M. N. Myers, *Sep. Sci. Technol.* **14**, 611 (1979).
35. M. Martin and P. Reynaud, *Anal. Chem.* **52**, 2293 (1980).
36. For exact work, Eqs. 5 and 6 must be corrected for the viscosity gradient accompanying dT/dx, which disturbs parabolic flow; see J. J. Gunderson, K. D. Caldwell, J. C. Giddings, *Sep. Sci. Technol.* **19**, 667 (1984).
37. K. D. Caldwell, L. F. Kesner, M. N. Myers, J. C. Giddings, *Science* **176**, 296 (1972).
38. J. C. Giddings, *J. Chromatogr.* **480**, 21 (1989).
39. K. D. Caldwell and Y. S. Gao, *Anal. Chem.*, in press.
40. J. C. Giddings and M. N. Myers, *Sep. Sci. Technol.* **13**, 637 (1978).
41. P. S. Williams, T. Koch, J. C. Giddings, *Chem. Eng. Commun.* **111**, 121 (1992).
42. R. G. Cox and H. Brenner, *Chem. Eng. Sci.* **23**, 147 (1968).
43. B. P. Ho and L G. Leal, *J. Fluid Mech.* **65**, 365 (1974).
44. R. G. Cox and S. K. Hsu, *Int. J. Multiphase Flow* **3**, 201 (1977).
45. S. K. Ratanathanawongs and J. C. Giddings, *Anal. Chem.* **64**, 6 (1992).
46. From Eq. 6, $(\Delta t_r/t^0) = w\Delta F/6kT$; a change ΔF in F of 10^{-17} N at $T = 300$ K with $w = 250$ μm thus shifts the retention time by $\Delta t_r = 0.106t^0$. Typically $t^0 \approx 1$ to 10 min, giving $\Delta t_r \approx 0.1$ to 1 min.
47. M. W. Chase, Jr., *et al.*, *J. Phys. Chem. Ref. Data* **14** (suppl. 1), 1 (1985).
48. J. C. Giddings, F. J. F. Yang, M. N. Myers, *Sep. Sci.* **10**, 133 (1975).
49. J. C. Giddings, G. Karaiskakis, K. D. Caldwell, M. N. Myers, *J. Colloid Interface Sci.* **92**, 66 (1983).
50. Particle-wall interactions affect retention for particles driven too close to the accumulation wall. Corrections must be applied or accuracy is compromised.
51. B. N. Barman and J. C. Giddings, *Langmuir* **8**, 51 (1992).
52. J. C. Giddings, G. Karaiskakis, K. D. Caldwell, *Sep. Sci. Technol.* **16**, 607 (1981).
53. K. D. Caldwell, G. Karaiskakis, M. N. Myers, J. C. Giddings, *J. Pharm. Sci.* **70**, 1350 (1981).
54. C. R. Yonker, K. D. Caldwell, J. C. Giddings, J. L. van Etten, *J. Virol. Methods* **11**, 145 (1985).
55. M. H. Moon and J. C. Giddings, *J. Pharm. Biomed. Anal.*, in press.
56. J. T. Li and K. D. Caldwell, *Langmuir* **7**, 2034 (1991).
57. R. Beckett, J. Ho, Y. Jiang, J. C. Giddings, *ibid.*, p. 2040.
58. B. Langwost and K. D. Caldwell, *Chromatographia* **34**, 317 (1992).
59. K. D. Caldwell, J. Li, J.-T. Li, *J. Chromatogr.* **604**, 63 (1992).
60. J. C. Giddings, F. J. Yang, M. N. Myers, *Science* **193**, 1244 (1976).
61. M.-K. Liu and J. C. Giddings, *Macromolecules*, in press.
62. M.-K. Liu, P. Li, J. C. Giddings, unpublished results.
63. S. K. Ratanathanawongs, unpublished results.
64. M. E. Schimpf and J. C. Giddings, *J. Polym. Sci. Polym. Phys. Ed.* **27**, 1317 (1989).
65. J. C. Giddings, M. E. Hovingh, G. H. Thompson, *J. Phys. Chem.* **74**, 4291 (1970).
66. M. E. Schimpf and J. C. Giddings, *J. Polym. Sci. Part B Polym. Phys.* **28**, 2673 (1990); M. E. Schimpf, L. M. Wheeler, P. F. Romeo, *ACS Symp. Ser.* **521**, 63 (1993).
67. M. N. Myers, P. Chen, J. C. Giddings, *ibid.*, p. 47.
68. J. J. Kirkland, S. W. Rementer, W. W. Yau, *Anal. Chem.* **60**, 610 (1988).
69. J. C. Giddings and M. H. Moon, *ibid.* **63**, 2869 (1991).
70. K. D. Caldwell and J. Li, *J. Colloid Interface Sci.* **132**, 256 (1989).
71. J. C. Giddings, F. J. Yang, M. N. Myers, *Anal. Biochem.* **81**, 395 (1977).
72. A. Litzén, J. K. Walter, H. Krischollek, K.-G. Wahlund, unpublished results.
73. L. E. Schallinger, W. W. Yau, J. J. Kirkland, *Science* **225**, 434 (1984).
74. E. C. Arner and J. J. Kirkland, *Biochim. Biophys. Acta* **993**, 100 (1989).
75. J. Lou, M. N. Myers, J. C. Giddings, unpublished results.
76. J. C. Giddings, F. J. Yang, M. N. Myers, *J. Virol.* **21**, 131 (1977).
77. K. D. Caldwell, T. T. Nguyen, J. C. Giddings, H. M. Mazzone, *J. Virol. Methods* **1**, 241 (1980).
78. K. D. Caldwell, G. Karaiskakis, J. C. Giddings, *J. Chromatogr.* **215**, 323 (1981).
79. S. M. Mozersky, K. D. Caldwell, S. B. Jones, B. E. Maleeff, R. A. Barford, *Anal. Biochem.* **172**, 113 (1988).
80. K. D. Caldwell, B. J. Compton, J. C. Giddings, R. J. Olson, *Invest. Ophthalmol. Visual Sci.* **25**, 153 (1984).
81. J. Gilbart, A. F. Wells, M. H. Hoe, A. Fox, *J. Chromatogr.* **387**, 428 (1987).
82. T. Sklaviadis, R. Dreyer, L. Manuelidis, *Virus Res.* **26**, 241 (1992).
83. K. D. Caldwell, G. Karaiskakis, J. C. Giddings, *Colloids Surf.* **3**, 233 (1981).
84. F.-S. Yang, K. D. Caldwell, M. N. Myers, J. C. Giddings, *J. Colloid Interface Sci.* **93**, 115 (1983).
85. R. A. Arlauskas, D. R. Burtner, D. H. Klein, *ACS Symp. Ser.* **521**, 2 (1993).
86. F.-S. Yang, K. D. Caldwell, J. C. Giddings, L. Astle, *Anal. Biochem.* **138**, 488 (1984).
87. J. C. Giddings, B N. Barman, M.-K. Liu, *ACS Symp. Ser.* **464**, 128 (1991).

88. K. D. Caldwell, Z.-Q. Cheng, P. Hradecky, J. C. Giddings, *Cell Biophys.* **6**, 233 (1984).
89. P. J. P. Cardot, J. Gerota, M. Martin, *J. Chromatogr.* **568**, 93 (1991).
90. A. Merino-Dugay, P. J. P. Cardot, M. Czok, M. Guernet, A. P. Andreux, *ibid.* **579**, 73 (1992).
91. A. Merino, C. Bories, J.-C. Gantier, P. J. P. Cardot, *ibid.* **572**, 291 (1991).
92. J. C. Bigelow, Y. Nabeshima, K. Kataoka, J. C. Giddings, *ACS Symp. Ser.* **464**, 146 (1991).
93. B. N. Barman, E. R. Ashwood, J. C. Giddings, *Anal. Biochem.*, in press.
94. S. Hoffstetter-Kuhn, T. Rösler, M. Ehrat, H. M. Widmer, *ibid.* **206**, 300 (1992).
95. J. C. Giddings, M. N. Myers, M. H. Moon, B. N. Barman, *ACS Symp. Ser.* **472**, 198 (1991).
96. M. H. Moon and J. C. Giddings, *Anal. Chem.* **64**, 3029 (1992).
97. J. C. Giddings, S. K. Ratanathanawongs, M. H. Moon, *KONA: Powder Particle* **9**, 200 (1991).
98. B. N. Barman, M. N. Myers, J. C. Giddings, *Powder Technol.* **59**, 53 (1989).
99. P. M. Shiundu, E. E. Remsen, J. C. Giddings, unpublished results.
100. M. A. Benincasa and J. C. Giddings, *Anal. Chem.* **64**, 790 (1992).
101. P. Sinclair, R. Beckett, B. T. Hart, *Hydrobiologia* **176/177**, 239 (1989).
102. R. Beckett and B. T. Hart, in *Environmental Particles*, J. Buffle and H. P. Van Leeuwen, Eds. (CRC Press, Boca Raton, FL, 1993), vol. 2, pp. 157–195.
103. G. Karaiskakis, K. A. Graff, K. D. Caldwell, J. C. Giddings, *Int. J. Environ. Anal. Chem.* **12**, 1 (1982).
104. R. Beckett, G. Nicholson, B. T. Hart, M. Hansen, J. C. Giddings, *Water Res.* **22**, 1535 (1988).
105. H. E. Taylor, J. R. Garbarino, D. M. Murphy, R. Beckett, *Anal. Chem.* **64**, 2035 (1992).
106. R. Beckett, D. M. Hotchin, B. T. Hart, *J. Chromatogr.* **517**, 435 (1990).
107. J. F. McCarthy, J. M. Zachara, *Environ. Sci. Technol.* **23**, 495 (1989).
108. D. J. Chittleborough, D. M. Hotchin, R. Beckett, *Soil Sci.* **153**, 341 (1992).
109. R. Beckett, Z. Jue, J. C. Giddings, *Environ. Sci. Technol.* **21**, 289 (1987).
110. R. Beckett, J. C. Bigelow, J. Zhang, J. C. Giddings, *Adv. Chem. Ser.* **219**, 65 (1989).
111. R. Beckett, F. J. Wood, D. R. Dixon, *Environ. Technol.*, in press.
112. R. V. Sharma, R. T. Edwards, R. Beckett, *Appl. Environ. Microbiol.*, in press.
113. This work was supported by grant CHE-9102321 from the National Science Foundation and Public Health Service grant GM10851-36 from the National Institutes of Health.

High-Resolution and Analytical Transmission Electron Microscopy of Mineral Disorder and Reactions

David R. Veblen, Jillian F. Banfield, George D. Guthrie, Jr., Peter J. Heaney, Eugene S. Ilton, Kenneth J. T. Livi, Eugene A. Smelik

Crystal defects and chemical reactions occurring at scales beyond the resolution of light microscopes have major effects on the chemical and physical properties of rocks and minerals. High-resolution imaging, diffraction, and chemical analysis in the transmission electron microscope have become important methods for exploring mineral defect structures and reaction mechanisms and for studying the distribution of phases resulting from reactions. These techniques have shown that structural disorder is common in some rock-forming minerals but rare in others. They have also established mechanisms by which many reactions occur at the atomic cluster scale. These data thus provide an atomistic basis for understanding the kinetics of geological reactions. Furthermore, apparent major-element, minor-element, and trace-element chemistry of minerals can be influenced by submicroscopic inclusions or intergrowths, which commonly form as products of solid-state reactions.

Transmission electron microscopy (TEM) has long been an important experimental technology in materials science, solid-state physics, and solid-state chemistry. Most processes of interest in these fields have analogs in the geological sciences, although the terminology used to describe them may differ. For example, materials scientists refer to degradation of metals as corrosion, whereas geochemists refer to mineral degradation occurring at Earth's surface as weathering. Annealing of metals is similar in many ways to contact metamorphism, and deformation of materials and rocks proceeds by the same mechanisms, although commonly at much different spatial and time scales. Indeed, much has been learned about the behavior of geological materials from experiments on metals, which typically exhibit much faster diffusion rates and deform plastically at much higher strain rates than most minerals.

Much can also be learned about solid-state materials from processes observed in minerals. Many rock-forming silicates have complex structures with relatively low symmetry (triclinic, monoclinic, or orthorhombic) and thus can provide an understanding of phase transformations in low-symmetry materials of technological interest. Although diffusion is sluggish in most silicates (zeolites and some clays excepted), geological time is immense compared with laboratory time scales, making minerals good analogs for materials processed for long periods. Among the thousands of mineral species are found the archetypes for many of our technologically vital materials. For example, the uncommon mineral perovskite ($CaTiO_3$) lends its name to the silicate perovskite structures such as high-pressure $MgSiO_3$, which are probably the most abundant minerals in the Earth's interior, as well as to numerous catalysts and ferroelectric materials, such as $BaTiO_3$. The perovskite structure is also the basis for many of the high-temperature superconductor structures, and the interest in structural variants, defects, and reactions in perovskite-based materials (*1*, *2*) spans the earth and materials science communities.

Just as TEM has revolutionized our understanding of the behavior of synthetic materials, these experimental tools are also being applied to the chemically complicated materials important in the earth sciences. Since the development of the quantitative analysis of fault displacements in the 1950s (*3*), conventional amplitude-contrast electron microscopy has made many fundamental contributions in the understanding of deformation mechanisms, in determining the textural relations between phase distributions, and in understanding processing conditions in metals and ceramics. By the mid-1970s geologists were routinely applying electron diffraction and conventional electron microscopy to similar problems in minerals (*4*). Indeed, amplitude-contrast imaging remains the primary method for examining both dislocations produced by deformation (*5*) and domain structures formed during phase transitions in minerals (*6*).

Great strides have been made during the past two decades in the development of TEM methods, including high-resolution TEM (HRTEM) and allied techniques, such as x-ray emission analytical transmission electron microscopy (AEM) (*7*) and convergent beam electron diffraction (CBED) (*8*). Furthermore, theoretical advances now make quantitative interpretation of results possible (*9*). Because these techniques are combined in many modern transmission electron micro-

D. R. Veblen and K. J. T. Livi are in the Department of Earth and Planetary Sciences, Johns Hopkins University, Baltimore, MD 21218. J. F. Banfield is in the Department of Geology and Geophysics, University of Wisconsin, Madison, WI 53706. G. D. Guthrie, Jr., is in the Earth and Environmental Sciences Division, Los Alamos National Laboratory, Los Alamos, NM 87545. P. J. Heaney and E. A. Smelik are in the Department of Geological and Geophysical Sciences, Princeton University, Princeton, NJ 08544. E. S. Ilton is in the Department of Geological and Environmental Sciences, Lehigh University, Bethlehem, PA 18015.